Analysis of Control Variables to Maximize Output Power for Switched Reluctance Generators in Single Pulse Mode Operation

Pairote Thongprasri and Supat Kittiratsatcha

Faculty of Engineering, King Mongkut's Institute of Technology Ladkrabang
Chalongkrung Road, Ladkrabang, Bangkok 10520, Thailand
sfengprt@src.ku.ac.th, kksupat@kmitl.ac.th

Abstract ─ This paper presents an analytical modeling method of optimal control variables to maximize the output power for switched reluctance generators (SRGs) in single pulse mode operation. A method to obtain the phase current equation used to determine the optimal control variables is proposed. The phase current equation is derived from the phase voltage equation in combination with the inductance model. The inductance model proposed in this paper is applied from the flux linkage function. The characteristics of the phase current and the energy conversion relations are analyzed to determine the optimal phase current shape. The analytical results indicate that the optimal shape can be generated when the SRG is controlled with the optimal control variables. The optimal shape is used for analysis based on the phase current equation to determine the optimal control variables. An 8/6 SRG experimental setup is used to validate the proposed method. The optimal control variables obtained from the proposed method are used to control the SRG. Based on the experimental results, the SRG can produce the maximum output power.

Index Terms ─ Control variables, optimal phase current shape, switched reluctance generator.

I. INTRODUCTION

A switched reluctance generator (SRG) is a potential candidate in various applications, such as an automotive starter/generator [1, 2] an engine starter/ generator [3, 4] and for variable speed wind energy [5] because it has a simple structure and low cost, is fault tolerant with a rugged structure, and involves easy starting/generating realization, high speed adaptability, with a high generation efficiency.

Its highly nonlinear nature is the main problem of the SRG, since the behavior of the SRG cannot be described by mathematical equations using conventional methods for a suitable controller design [6]. The SRG model is used for simulation to determine the relationship between output power and control variables since there is no analytical equation with which to determine the output power based on design parameters and control variables [7]. The dynamic model of an SRG using a cubic spline technique has been proposed to find the flux linkage, inductance, torque, and output power [8]. A model SRG based on the Finite Element Method (FEM) and power control methods for a small wind power generation system has been proposed in [9]. The SRG model is used to find the output power curve versus the shaft speed. This curve is analyzed to determine the optimal switching on-off angle for maximum efficiency in the system.

The output power of the SRG in single pulse mode can be controlled by adjusting the excitation angles, with the turn-on/off angle being fixed while the turn-off/on angle is adjusted, or by adjusting both the turn-on and turn-off angles. Constant output power control of the SRG has been proposed by controlling the turn-on angle with a fuzzy logic algorithm while the turn-off angle is fixed [10]. The optimal excitation angles for output power control using automatic closed loop control have been proposed so that the optimal turn-off angle in terms of power and speed is determined from an analytical fit curve [11], while the optimal turn-on angle is automatically adjusted based on the closed loop power control to regulate the output power. The optimal excitation angles have been proposed for maximum system efficiency calculated using the ratio of the two flux linkages [12]. The minimum torque ripple occurs in this case. With two flux linkages, one is the position at which the stator and rotor pole corners begin overlap and the other is the position at maximum value. A Modified Angle Position Control (MAPC) method has been proposed to determine the optimal shape of the phase current [13]. The optimal turn-on angle is fixed and the optimal turn-off angle can be determined by the analytical model of the SRG for the maximum energy conversion [14, 15].

A mathematical model for analyzing control variables and describing the behavior of the SRG and the flux linkage versus current characteristics calculation is essential. There are at least two methods to obtain flux linkage versus current characteristics—an analytical approach based on the FEM and an experimental

Submitted On: November 28, 2015
Accepted On: July 17, 2016

1054-4887 © ACES

approach based on direct measurements. The flux linkage model based on the FEM has well known reliability, however it requires intensive computation and many details of the machine geometry and structure [16]. Analytical nonlinear models of flux linkage have been described in [17-20] that are accurate and reliable. The model based on machine geometry introduced in [17] is complicated and depends on flux linkage at aligned and unaligned positions, and a position-dependent function. The position-dependent term has a physical significance in that its coefficient needs to be related to the machine geometry. The model proposed in [18] is a little complex because the flux linkage curve is divided into 2 parts, namely, linear and nonlinear. However, it only requires the flux linkage versus current characteristics at the aligned and unaligned positions. The model described in [19] based on a Fourier series with a limited number of terms is complex since it is necessary to know the flux linkage versus current characteristics at the aligned, unaligned, and midway positions. The coefficients in terms of the Fourier series depend on the flux linkage positions at aligned, unaligned, and midway positions so that the flux linkage at the aligned and midway positions can be calculated via curve fitting based on an arc-tangent function. The Stiebler model proposed [20] is simple in that it is composed of an angular function and aligned and unaligned flux linkage. However, it is proposed in a per-unit system.

An analytical modeling method of the optimal control variables to maximize the output power of the SRGs in single pulse mode operation is presented in this paper. The control variables comprise a dc bus voltage, a shaft speed or angular velocity, and excitation angles. This paper proposes a method to obtain the phase current equation used to determine the optimal control variables. The phase current equation is derived from the phase voltage equation in combination with the inductance model. The proposed inductance model in a real system is applied from the flux linkage function in a per-unit system introduced by Stiebler. It requires the geometrical parameters of an SRG at the aligned and unaligned rotor positions. These parameters are easily quantified using the FEM. The optimal phase current shape depending on the control variables is investigated to determine the optimal shape. Finally, the optimal shape of the phase current is used to determine the optimal control variables. An 8/6 SRG experimental setup is used to verify the proposed method.

II. PRINCIPLE OF SRG IN SINGLE PULSE MODE OPERATION

A 4-phase 8/6 SRG is used in this paper which is driven by a 4-phase asymmetrical bridge converter as shown in Fig. 1. When S_A and $S_{A'}$ are both on, the phase A voltage is u. If S_A and $S_{A'}$ are both off, the phase A voltage is $-u$.

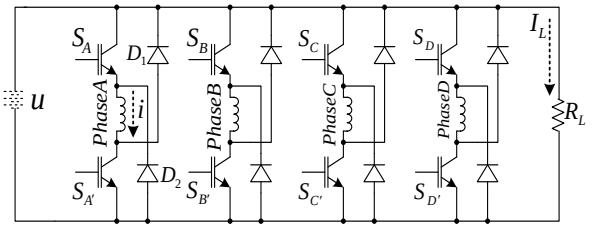

Fig. 1. 4-phase asymmetrical bridge converter.

The mutual inductance between individual phases of the SRG is usually neglected. Therefore, the equation of voltage for each phase of SRG is expressed as:

$$u = Ri + \frac{d\lambda(i,\theta)}{dt}. \tag{1}$$

The voltage equation at constant speed is given by:

$$u = Ri + L(\theta)\frac{di}{dt} + e, \tag{2}$$

where u represents the dc bus voltage, i is the phase current, R and L are the phase of resistance and inductance, respectively, ω is the angular velocity, and the back emf is defined as:

$$e = i\omega\frac{\partial L(i,\theta)}{\partial\theta}. \tag{3}$$

The energy converted is the area enclosed by the loci which is expressed as:

$$W = \oint \lambda di = \oint id\lambda. \tag{4}$$

The SRG requires an excitation source in order to generate electrical energy. The SRG (phase A) is excited by the asymmetrical bridge converter as shown in Fig. 2. This converter is used as the dc source [21] for the exciting phase A of the SRG through two switches as shown in Fig. 2 (bottom) and demagnetizing the same phase through two diodes as shown in Fig. 2 (top).

In Fig. 2, the current builds in the SRG phase winding when the controllable switches are closed and no energy is supplied to the load. When the controllable switches are opened, the stored energy is supplied to the load through the two diodes. The average load current can be defined as:

$$I_L = \frac{1}{2\pi/N_r}\left(\int_{\theta_{off}}^{\theta_e} id\theta - \int_{\theta_{on}}^{\theta_{off}} id\theta\right), \tag{5}$$

where turn-on θ_{on} and turn-off θ_{off} angles represent the controllable switches which are closed and opened, respectively, θ_e is the angle at which the phase current is depleted and it is given as $2\theta_{off} - \theta_{on}$, θ is the rotor position and N_r is the number of rotor poles.

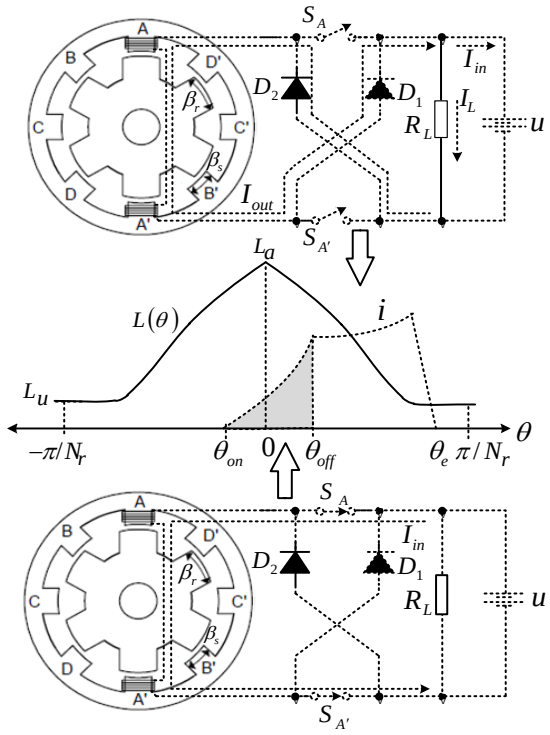

Fig. 2. Power generation process for the SRG in single pulse mode.

The average electric power of the SRG is the summation of the output power of each phase in one revolution which is given by:

$$P_{out} = I_L u . \tag{6}$$

The main electrical losses of an SRG are copper loss and iron loss. The copper loss P_{Cu} depends on the rms phase current I_{rms} on the range $\theta_{off} \le \theta \le \theta_e$ [22] which is expressed as:

$$P_{Cu} = N_{ph} I_{rms}^2 R , \tag{7}$$

and

$$I_{rms}^2 = \frac{1}{2\pi / N_r} \int_{\theta_{off}}^{\theta_e} i^2 d\theta . \tag{8}$$

The iron loss is in proportion to the excitation magnetic motive force and the stroke frequency. It is not uniformly distributed in the core since the flux shape is non-sinusoidal and the flux harmonic spectrum differs in various parts of the magnetic spectrum. The iron loss [23] can be approximately calculated as:

$$P_C = K_h f B_m^{a+bB_m} + K_e f^2 B_m^2 , \tag{9}$$

where f is the stroke frequency, K_h and K_e are the hysteresis and eddy-current loss coefficients, respectively, a and b are the constants of the exponent, and B_m is the amplitude of flux density for sinusoidal variation.

III. ANGLE POSITION CONTROL METHOD

The control variables of the SRG are the dc bus voltage u, the angular velocity ω, the phase current i, and turn-on/off angle $\theta_{on} / \theta_{off}$. The Angle Position Control (APC) method can control the phase current shape by adjusting θ_{on} and θ_{off} while u and ω are constant. The output power can be adjusted by the phase current. The advantages of the APC method [13] are that the optimal θ_{on} and θ_{off} can improve efficiency, the multiple phases can be conducted at the same time, and the torque adjustment range is wide.

The effect of θ_{on} and θ_{off} on the phase current shape using the APC method is illustrated in Fig. 3, where θ_{on} is fixed and θ_{off} is adjusted as shown in Fig. 3 (a) and θ_{off} is fixed and θ_{on} is adjusted as shown in Fig. 3 (b).

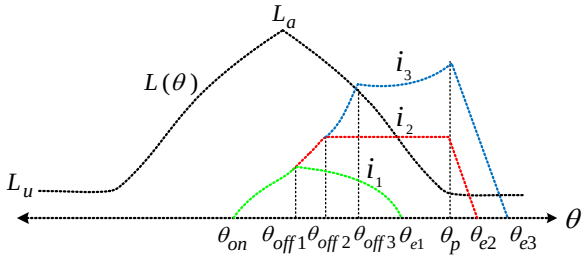

(a) θ_{on} is fixed and θ_{off} is adjusted

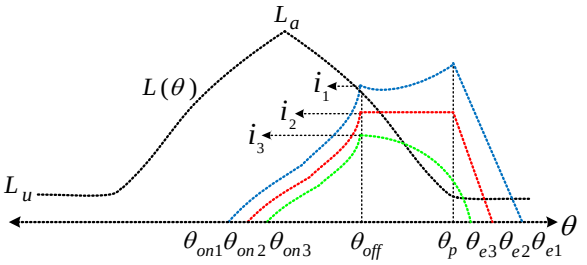

(b) θ_{off} is fixed and θ_{on} is adjusted

Fig. 3. Phase current shapes using the angle position control method.

When the resistance of the phase windings and the voltage drops of the main switches and diodes are neglected, the voltage Equation in (2) can be expressed as:

$$u = \omega L(\theta) \frac{di}{d\theta} + \omega i \frac{\partial L(i,\theta)}{\partial \theta} . \tag{10}$$

The maximum value of the phase current in Fig.

4 is in the range $\theta_{off} \le \theta \le \theta_p$ and θ_p equals $(\beta_r + \beta_s)/2$, where β_r is the rotor pole arc and β_s is the stator pole arc. Considering (10), if the back emf is smaller than the dc bus voltage, then $di/d\theta < 0$. The phase current shape in this case is shown in Fig. 4 (a). If the back emf is equal to the dc bus voltage, then $di/d\theta = 0$. In this case, the phase current shape is shown in Fig. 4 (b). If the back emf is bigger than the dc bus voltage, then $di/d\theta > 0$ and the phase current shape is shown in Fig. 4 (c).

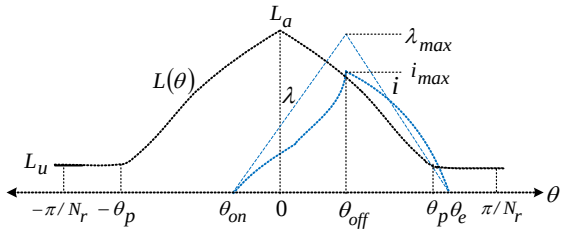

(a) Back emf is smaller than dc bus voltage

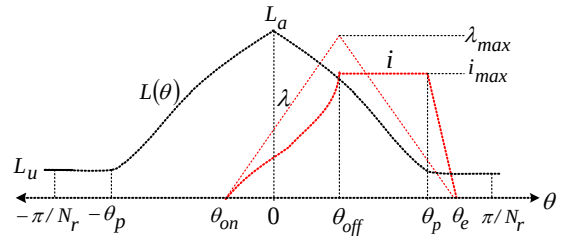

(b) Back emf is equal to dc bus voltage

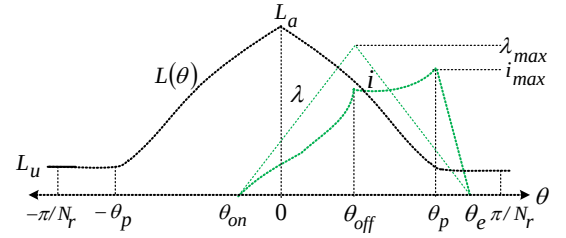

(c) Back emf is bigger than dc bus voltage

Fig. 4. Three kinds of phase current and flux linkage at different turn-on and turn-off angles with the same maximum value of the phase current.

From (9), the iron loss depends on the maximum flux linkage. The maximum value of the flux linkage in Fig. 4 occurs for θ_{off}. The copper loss depends on the rms phase current which can be quantified by (7).

The energy conversion loops for 3 kinds of i and λ by the loci are shown in Fig. 5. The maximum output power can be produced when the phase current is controlled in the shape of a flat top (Fig. 4 (b)). This result has been confirmed by [24].

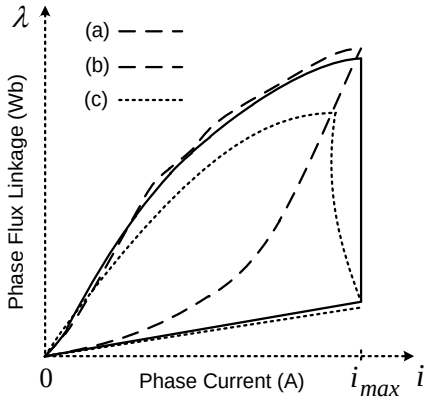

Fig. 5. Energy conversion loops by the loci with the same maximum value of the phase current.

IV. PROPOSED METHOD FOR ANALYZING THE OPTIMAL CONTROL VARIABLES

An analytical modeling method of the optimal control variables to maximize output power of the SRGs in single pulse mode operation is presented in this paper. This paper proposes a method to obtain the phase current equation used to determine the optimal control variables. The phase current equation will be derived from the phase voltage equation in combination with the inductance model. The inductance model is applied from the flux linkage function. Finally, the optimal shape of the phase current is used to determine the optimal control variables.

A. Flux linkage model

The flux linkage model in a real system as shown in Fig. 6 has been developed from the flux linkage function in a per-unit system introduced by Stiebler [20]. It requires the geometrical parameters of an SRG at the aligned and unaligned rotor positions. These parameters are easily determined using an experiment or the FEM. The parameters comprise inductance at positions of aligned L_a and unaligned L_u, and flux linkage at points s and m as shown in Fig. 6.

The flux linkage function in Fig. 6 is composed of the linear and saturated regions. The saturated region begins at point s and finishes at point m. The flux linkage of the saturated region can be determined using a Froelich function [25] $\lambda = (i/(a+b))$, where a and b are constants as the slope and intercept, respectively. The constants a and b can be determined by substituting the λ_{as}, i_s of the point s and λ_{am}, i_m of the point m into the Froelich function.

The proposed model of the flux linkage can be

expressed as:

$$\lambda(i,\theta) = L_u i + (L_a - L_u)\frac{i}{a+bi} f(\theta), \qquad (11)$$

where θ_k is the effective overlap position of the stator and rotor poles, and the angular function is given by:

$$f(\theta) = \begin{cases} 0.5 + 0.5\cos\left(\theta \dfrac{\pi}{\theta_k}\right) & ,-\theta_k \le \theta \le \theta_k \\ 0 & ,else \end{cases}. \qquad (12)$$

To verify the proposed method, an 8/6 SRG is used to determine its geometrical parameters using the FEM with its specifications as shown in Table 1.

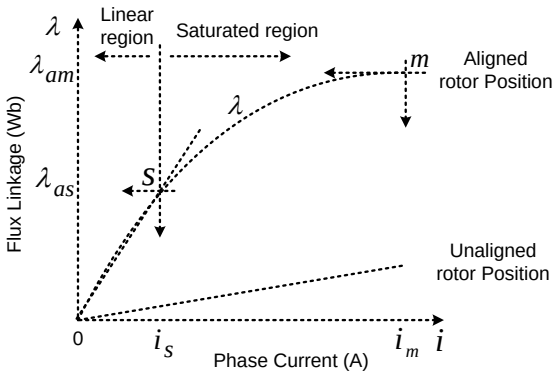

Fig. 6. Magnetization curve of an SRG.

Table1: Specifications of the candidate SRG

Parameter	Value
Outer diameter of stator	150 mm
Inner diameter of stator	70 mm
Stack length	72 mm
Length of air gap	0.5 mm
Number of phases	4
Stator/Rotor pole arc	23°/23.5°
Number of stator poles/rotor poles	8/6
Rated voltage/power/speed	48 V/2.3 kW/ 6000 rpm

The relationship between the flux linkage and current at rotor positions 0°, 15°, and 30° is obtained using the FEM and are shown in Table 2.

The parameters obtained using the FEM for calculation in this paper consist of L_a = 470 μH, L_u = 42 μH, θ_k = 27°, a = 0.65, and b = 0.155.

Figure 7 shows the resultant magnetization curve at rotor positions 0°, 15°, and 30° obtained from the analytical model (11) compared with the FEM which demonstrates the validity of the proposed model.

Table 2: Analytical results obtained using the FEM

Current (A)	Rotor Position (Mech. Degree)		
	0°	15°	30°
50	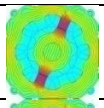	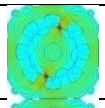	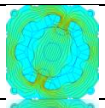
40	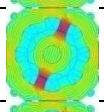	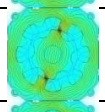	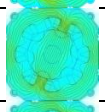
30	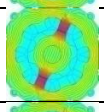	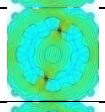	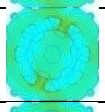
20	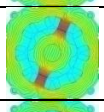	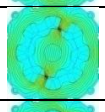	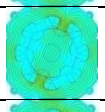
10	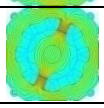	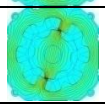	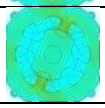

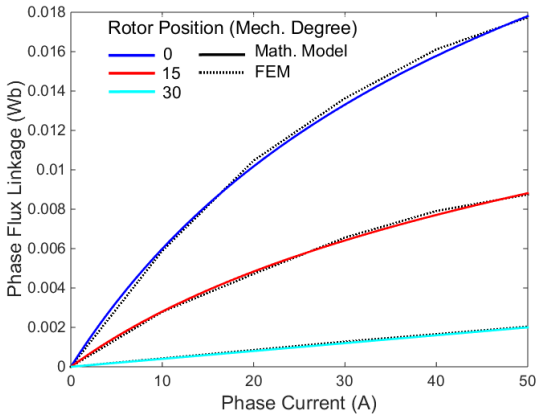

Fig. 7. Magnetization curves of the candidate SRG at rotor positions 0°, 15°, and 30° obtained using the analytical model (solid lines) and the FEM (dotted lines).

B. Proposed model of phase current

The phase inductance involves much more than a comparison with the mutual inductance, as the mutual inductance is neglected [26, 27]. It is known by $L(i,\theta) = \lambda(i,\theta)/i$. Therefore, based on (11) and (12), the phase inductance is;

$$L(i,\theta) = L_u + \frac{L_a - L_u}{a+bi} f(\theta), \qquad (13)$$

where the angular function $f(\theta)$ is in the range $-\theta_k \le \theta \le \theta_k$.

The inductance profile is a periodic function with period of $2\pi / N_r$ or the rage from $-\pi / N_r$ to π / N_r. Consequently, the phase inductance model proposed in this paper is divided into three regions depending on the

phase current and rotor position as shown in Fig. 8. It can be expressed as:

$$L(i,\theta)=\begin{cases} L_u & ,-\dfrac{\pi}{N_r}\le\theta<-\theta_k \\ L_u+\dfrac{L_a-L_u}{a+bi}f(\theta) & ,-\theta_k\le\theta\le\theta_k \\ L_u & ,\theta_k<\theta\le\dfrac{\pi}{N_r} \end{cases} \quad .(14)$$

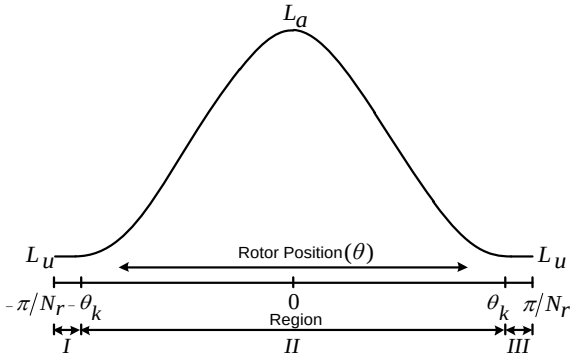

Fig. 8. Phase inductance profile is divided into three regions.

Figure 9 depicts the phase inductance of the candidate SRG obtained using the proposed analytical model (14) and the FEM so that the characteristics of the phase inductance versus the current and rotor position closely match each other.

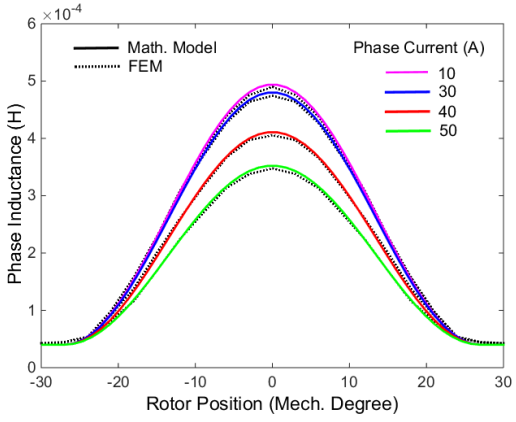

Fig. 9. Phase inductance of the candidate SRG obtained using the mathematical model and the FEM.

The expression of the phase current is obtained by substituting the inductance model (14) into the phase voltage Equation (10). It can be expressed as:

$$i=\begin{cases} \dfrac{u(\theta-\theta_{on})}{\omega\left[L_u+\left(\dfrac{L_a-L_u}{a+bi}\right)f(\theta)\right]} & ,\theta_{on}\le\theta<\theta_{off} \\ \dfrac{u(\theta_e-\theta)}{\omega\left[L_u+\left(\dfrac{L_a-L_u}{a+bi}\right)f(\theta)\right]} & ,\theta_{off}\le\theta\le\theta_e \\ 0 & ,else \end{cases} \quad .(15)$$

The phase torque is given by:

$$T(i,\theta)=\frac{1}{2}i^2\frac{\partial L(i,\theta)}{\partial\theta}$$

$$=\left(\frac{(a+bi)f'(\theta)+bf(\theta)\left((L_a-L_u)f(\theta)i+\dfrac{u}{\omega}b\right)+c}{(2bL_u+d)(a+bi)^2}\right)\times(L_a-L_u)i^2, \quad (16)$$

where

$$c=u\begin{cases} -a & ,\theta_{on}\le\theta<\theta_{off} \\ a & ,\theta_{off}\le\theta\le\theta_e \\ 0 & ,else \end{cases},$$

$$d=aL_u+(L_a-L_u)f(\theta)-\frac{b}{\omega}h,$$

$$h=\frac{u}{\omega}\begin{cases} u(\theta-\theta_{on}) & ,\theta_{on}\le\theta<\theta_{off} \\ u(\theta_e-\theta) & ,\theta_{off}\le\theta\le\theta_e \\ 0 & ,else \end{cases}.$$

C. Analysis of optimal control variables

To obtain the maximum output power, the optimal control variables are required from Equation (15) as mentioned in the previous topic. The maximum value of the phase current in Fig. 4 can occur when θ is in the range $\theta_{off}\le\theta\le\theta_p$. Therefore, the maximum value of the phase current based on (15) can be given as:

$$i_{\max}=\frac{u(\theta_e-\theta)}{\omega\left[L_u+\left(\dfrac{L_a-L_u}{a+bi_{\max}}\right)f(\theta)\right]}. \quad (17)$$

The maximum output power can be produced when the phase current is controlled in the shape of a flat top

as shown in Fig. 4 (b). This result has been confirmed by [24]. Therefore, the shape of the phase current in Fig. 4 (b) is used to determine the optimal control variables so that the maximum value exists in the interval θ_{off} to θ_p.

The maximum value of the phase current at $\theta = \theta_{off}$ or $i_{\max 1}$ can be known by substituting $\theta = \theta_{off}$ into (17) which is given by:

$$i_{\max 1} = \frac{u(\theta_{off} - \theta_{on})}{\omega\left[L_u + \left(\frac{L_a - L_u}{a + bi_{\max 1}}\right)\left(\frac{1}{2} + \frac{1}{2}\cos\left(\theta_{off}\frac{\pi}{\theta_k}\right)\right)\right]}. \quad (18)$$

Furthermore, the maximum value of the phase current at $\theta = \theta_p$ or $i_{\max 2}$ can be determined by substituting $\theta = \theta_p$ into (17) which is expressed as:

$$i_{\max 2} = \frac{u(2\theta_{off} - \theta_{on} - \theta_p)}{\omega\left[L_u + \left(\frac{L_a - L_u}{a + bi_{\max 2}}\right)\left(\frac{1}{2} + \frac{1}{2}\cos\left(\theta_p\frac{\pi}{\theta_k}\right)\right)\right]}. \quad (19)$$

Now $i_{\max 1}$ is equal to the $i_{\max 2}$ since the shape of phase current is flat topped. The optimal turn-on angle can be calculated by substituting $i_{\max 1}$ into $i_{\max 2}$.

Consequently,

$$\theta_{on}^{opt} = \frac{\theta_{off}^{opt}(L_u + 2qf_1(\theta) - qf_2(\theta)) - \theta_3(L_u + qf_1(\theta))}{q(f_1(\theta) - f_2(\theta))}, \quad (20)$$

where

$$q = \frac{L_a - L_u}{a + bi_{\max}},$$

$$f_1(\theta) = 0.5 + 0.5\cos\left(\theta_{off}^{opt}\frac{\pi}{\theta_k}\right),$$

$$f_2(\theta) = 0.5 + 0.5\cos\left(\theta_p\frac{\pi}{\theta_k}\right).$$

Based on (15) in the range $\theta_{off} \le \theta \le \theta_p$, the position of θ at the maximum current point can be determined by $\frac{di}{d\theta} = 0$:

$$\pi(L_a - L_u)\sin\left(\theta\frac{\pi}{\theta_k}\right) = 2\left(\frac{u}{\omega}\right)\theta_k(a + bi_{\max}). \quad (21)$$

Then, the optimal turn-off angle can be found by substituting θ_{off} into θ:

$$\theta_{off}^{opt} = \frac{\theta_k}{\pi}\sin^{-1}\left(\frac{2u\theta_k}{\omega\pi(L_a - L_u)}(a + bi_{\max})\right). \quad (22)$$

Ultimately, as θ_p, u, and $i_{\max}$ are defined, the control variables of the SRG for maximum output power can be calculated as follows:

i. The angular velocity ω can be determined by substituting values of u, $i_{\max}$, and $\theta = \theta_p$ into (21).
ii. The value of θ_{off}^{opt} can be found by applying the values of θ_p, u, $i_{\max}$, and ω into (22).
iii. The value of θ_{on}^{opt} can be determined from (20).

V. ANALYTICAL AND EXPERIMENTAL RESULTS

To verify the proposed method, an 8/6 SRG system is set up as shown in Fig. 10. A 3-phase induction motor is used as the prime mover so that its speed is controlled by an inverter. The parameters of the SRG are shown in Table 1. A battery rated at 12 V and 120A is used as the constant dc bus voltage u. The average torque T_m of the prime mover is measured by a rotational torque transducer which is connected between the prime mover and the SRG. The shaft speed or angular velocity ω and aligned position θ_a are detected by a resolver mounted on the SRG. The SRG is driven by a 4-phase asymmetrical bridge converter so that excitation angles are created by a TMS320F28027. The R_L equals 1.25 Ω and is used as the resistive load.

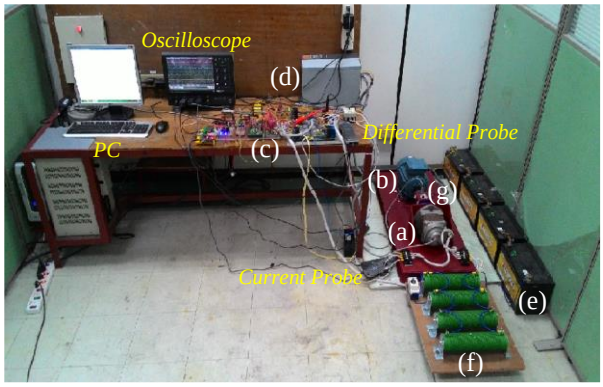

Fig. 10. Experimental setup: (a) 8/6 SRG with a resolver, (b) prime mover, (c) asymmetrical bridge converter and TMS320F28027 DSP controller, (d) variable speed inverter, (e) 12 V, 120 A battery, (f) resistive load, and (g) torque meter.

Figure 11 shows the schematic layout of the experimental setup so that the mechanical input power can be calculated by:

$$P_{in} = T_m \omega . \quad (23)$$

The efficiency of the system is defined as:

$$\eta = \frac{P_{out}}{P_{in}}, \quad (24)$$

where P_{out} is the electrical output power and P_{in} is the mechanical input power.

In this paper, the parameters used for analysis comprise $L_u = 42\ \mu H$, $L_a = 470\ \mu H$, $\beta_s = 23°$, $\beta_r = 23.5°$, $a = 0.65$, and $b = 0.155$.

The relationship between the system efficiency of the SRG and the 3 kinds of phase current are investigated, if the P_{out}, u, and θ_{off} are defined as 1000 W, 36 V, and 9°, respectively, the I_L equals to 27.78 A obtained from (6). Analytical results based on the mathematical models (5), (8), (11), and (15) and Figs. 12-14 show the power generation waveforms when the turn-on angle and angular velocity have been adjusted to control I_L = 27.78 A. The values of θ_{on}, θ_{off}, ω, $i_{\max}$, λ_{max}, and I_{rms} are summarized in Table 3.

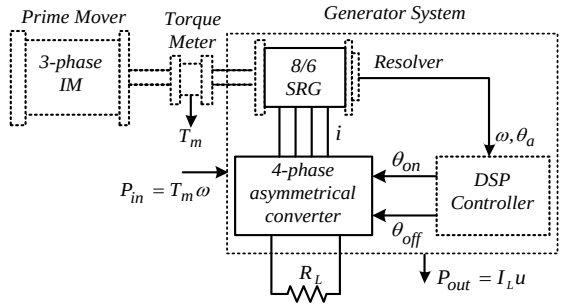

Fig. 11. Schematic layout of the experimental setup.

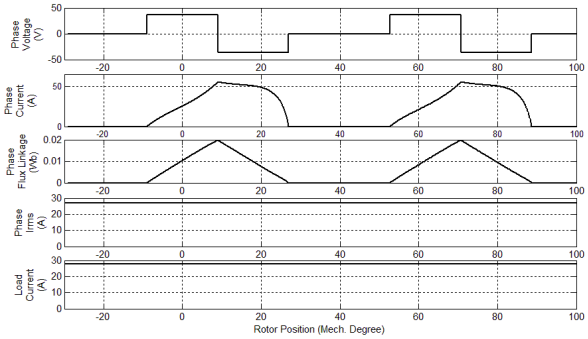

Fig. 12. Case 1: θ_{on} and θ_{off} are -9.20° and 9°.

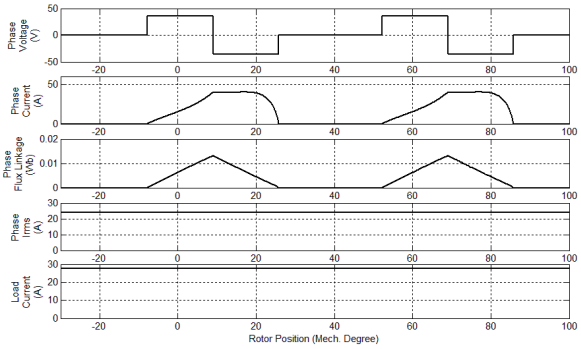

Fig. 13. Case 2: θ_{on} and θ_{off} are -7.80° and 9°.

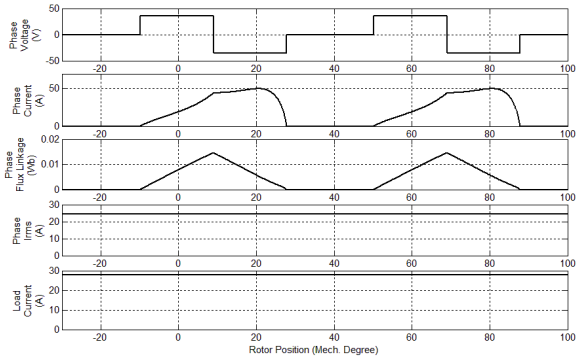

Fig. 14. Case 3: θ_{on} and θ_{off} are -8.15° and 9°.

Table 3: Results obtained from analytical model

Case	θ_{on} (°)	θ_{off} (°)	ω (rad/s)	$i_{\max}$ (A)	$\lambda_{\max}$ (Wb)	I_{rms} (A)
1	-9.20	9	524	55	0.0193	26.81
2	-7.80	9	586	40	0.0132	23.85
3	-8.15	9	605	50	0.0145	24.54

Based on (7) and (9), the copper loss and iron loss depend on I_{rms} and λ_{max}, respectively. In Table 3, the maximum efficiency of the system occurs in case 2 since the copper loss and iron loss are lowest.

The experimental results in Figs. 15-17 show the waveforms of the average torque of the prime mover, phase current, dc bus voltage, and load current. Their values are summarized in Table 4.

The efficiency of the system can be determined using (24). In Table 4, the maximum efficiency of the system occurs in case 2 where the shape of the phase current is flat topped. This result corresponds with the result obtained from the proposed analytical model.

The relationship between the output power of the SRG and the 3 kinds of phase current is investigated

where the maximum value of the 3 kinds of the phase current is controlled at 40 A by adjusting the control variables. The analytical results, the shapes of the phase inductance, phase flux linkage, phase current, phase torque, and load current obtained from analytical models (14), (11), (15), and (16), respectively, are shown in Figs. 18 (a)-(c). The energy conversion loops are shown in Fig. 18 (d) with the maximum output power occurring in case b. In this case, the phase current shape is flat topped. The control variables are summarized in Table 5.

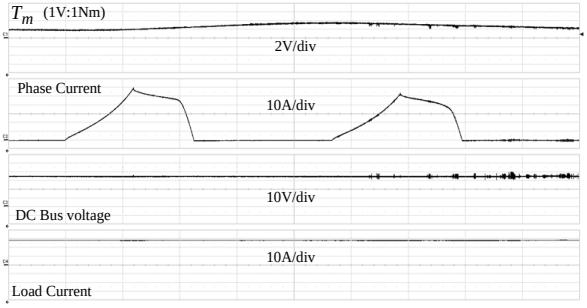

Fig. 15. Case 1: $i_{\max}$= 55 A, θ_{on} and θ_{off} are -9.20° and 9°.

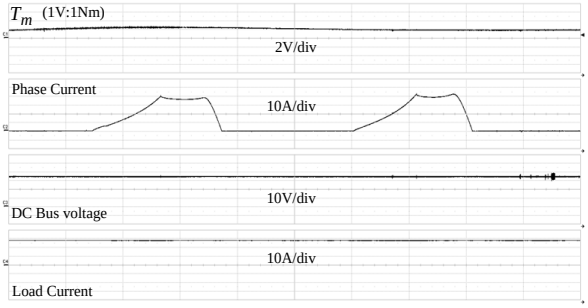

Fig. 16. Case 2: $i_{\max}$= 40 A, θ_{on} and θ_{off} are -7.80° and 9°.

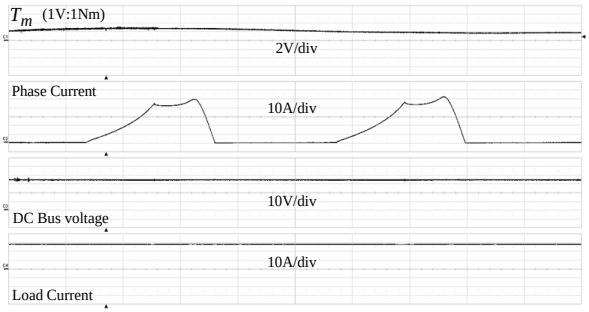

Fig. 17. Case 3: $i_{\max}$= 50 A, θ_{on} and θ_{off} are -8.15° and 9°.

Table 4: System efficiency obtained by 3 kinds of i

Case	ω (rad/s)	T_m (Nm)	P_{in} (W)	u (V)	I_L (A)	P_{out} (W)	η (%)
1	524	2.58	1351.9	36.2	26.7	965.5	71.4
2	586	2.04	1195.4	36.1	26.8	967.5	80.9
3	605	2.11	1276.6	36.3	26.6	965.6	75.6

Table 5: Three cases of control variables

Case	u (V)	ω (rad/s)	$i_{\max}$ (A)	θ_{on} (°)	θ_{off} (°)	I_L (A)	P_{out} (W)
a	36	513	40	-7.8	5.5	16.70	601.2
b	36	586	40	-7.8	9	27.80	1000.8
c	36	648	40	-7.8	9.5	24.68	888.5

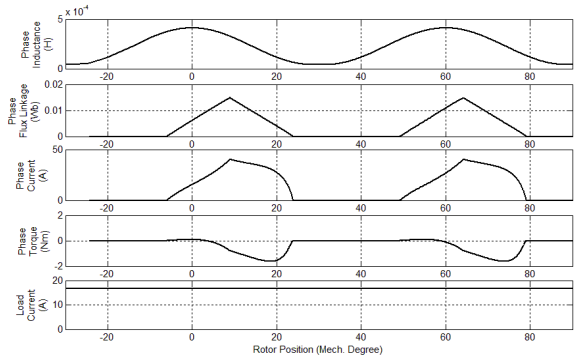

(a) Case a: θ_{on} = -7.8° and θ_{off} = 5.5°

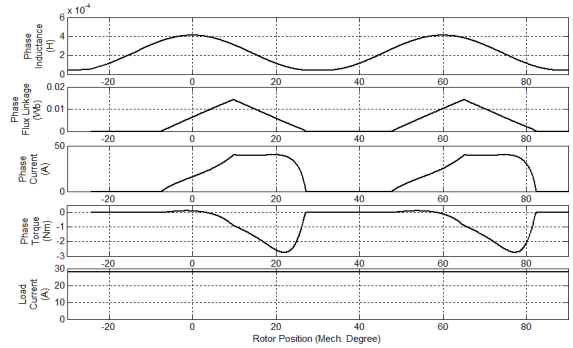

(b) Case b: θ_{on} = -7.8° and θ_{off} = 9°

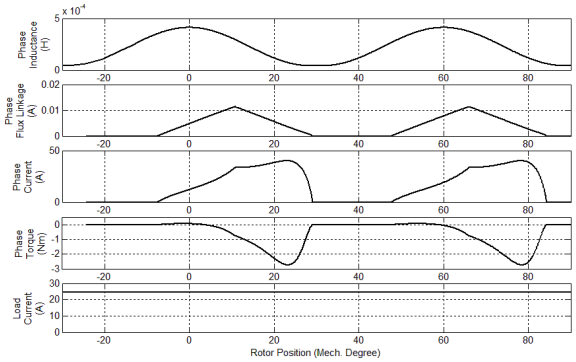

(c) Case c: θ_{on} = -7.8° and θ_{off} = 9.5°

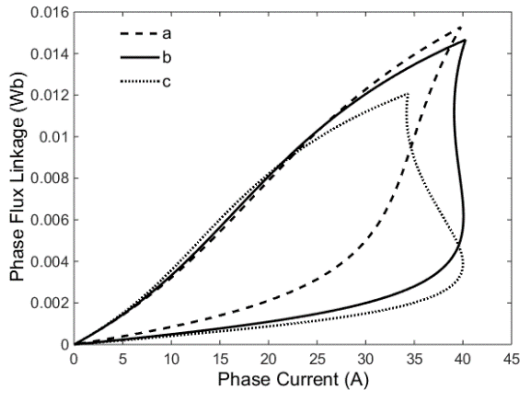

(d) Three cases of energy conversion loop

Fig. 18. Relationship between P_{out} and 3 kinds of i.

The experimental results in Fig. 19 show the waveforms of the phase voltage, phase current, dc bus voltage, and load current. The 3 cases of output power are: case a = 582.8 W, case b = 967.5 W, and case c = 857.9 W. The output power obtained from the measurement is less than the output power obtained from the analytical model since the resistance of the phase windings in the analytical model is neglected. The SRG can produce the maximum output power in case b so that this result corresponds with the analytical result.

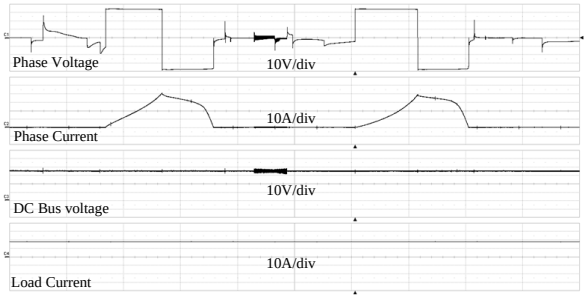

(a) Case a: $i_{\max} = 40$ A, $\theta_{on} = -7.8°$, $\theta_{off} = 5.5°$, $I_L = 16.1$ A, and $u = 36.2$ V

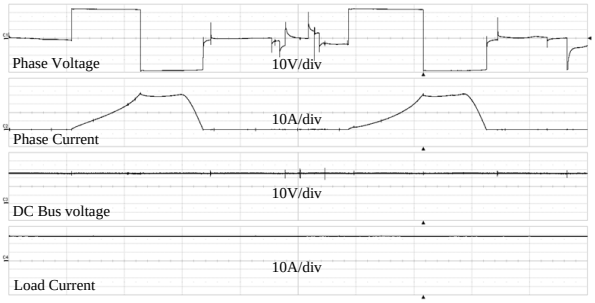

(b) Case b: $i_{\max} = 40$ A, $\theta_{on} = -7.8°$, $\theta_{off} = 9°$, $I_L = 26.8$ A, and $u = 36.1$ V

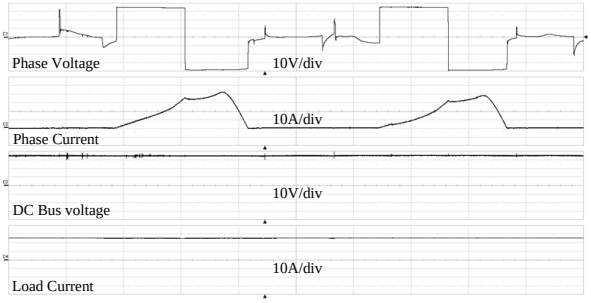

(c) Case c: $i_{\max} = 40$ A, $\theta_{on} = -7.8°$, $\theta_{off} = 9.5°$, $I_L = 23.7$ A, and $u = 36.2$ V

Fig. 19. Relationship between P_{out} and 3 kinds of i at the same maximum value based on measurement.

To maximize the output power, the optimal control variables ω, θ_{off}^{opt}, and θ_{on}^{opt} can be calculated as follows:

i. The angular velocity ω can be determined by substituting u, $i_{\max}$, and $\theta = \theta_p$ into (21).
ii. The value of θ_{off}^{opt} can be found by using the values of θ_p, u, $i_{\max}$, and ω in (22).
iii. The value of θ_{on}^{opt} can be determined from (20).

Table 6 shows the control variables obtained by the proposed model where θ_p, u, and $i_{\max}$ are defined as: $\theta_p = 23.25°$, $u = 24$ V, 36 V, and 48 V, and $i_{\max} = 30$ A, 40 A, and 50 A.

Table 6: Control variables using the proposed model

Case	θ_p (°)	u (V)	$i_{\max}$ (A)	ω (rad/s)	θ_{on} (°)	θ_{off} (°)	I_L (A)
i	23.25	24	30	547	-7.2	8.8	19.59
ii	23.25	36	40	586	-7.8	9	27.8
iii	23.25	48	50	628	-8.4	9.2	39.76

The analytical results for the three cases, the shapes of the phase A voltage, phase A current, phase B current, and the load current obtained from analytical model are shown in Fig. 20. The shape of the phase current in all cases is flat-topped because the SRG is controlled using the optimal variable controls.

The experimental results in Fig. 21 show the waveforms of the phase A voltage, phase A current, Phase B current, and load current. The 3 cases of output power are: case i = 454.9 W, case ii = 967.5 W, and case iii = 1841.2 W.

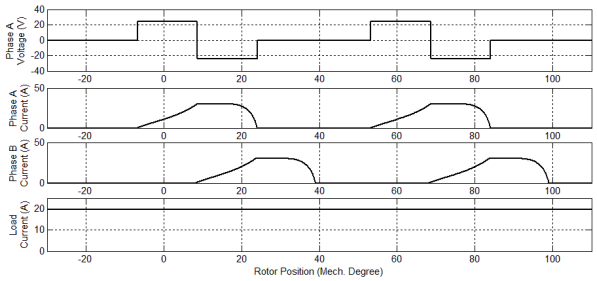

(a) Case i: θ_{on} = -7.7°, θ_{off} = 8.8°, and I_L = 19.59 A

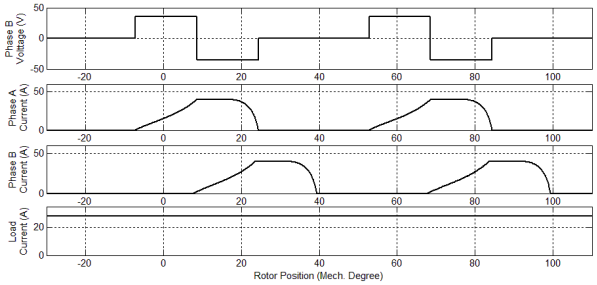

(b) Case ii: θ_{on} = -7.8°, θ_{off} = 9°, and I_L = 27.8 A

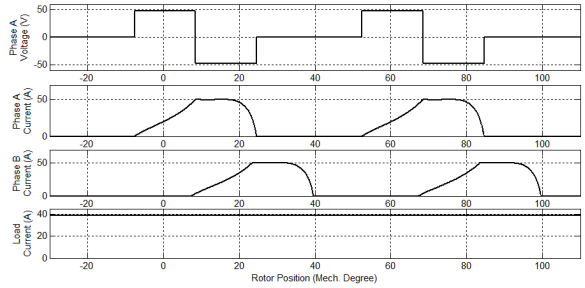

(c) Case iii: θ_{on} = -8.4°, θ_{off} = 9.2°, and I_L = 39.76 A

Fig. 20. Three cases for waveforms of the phase current, when the SRG is controlled with the control variables obtained from the analytical model.

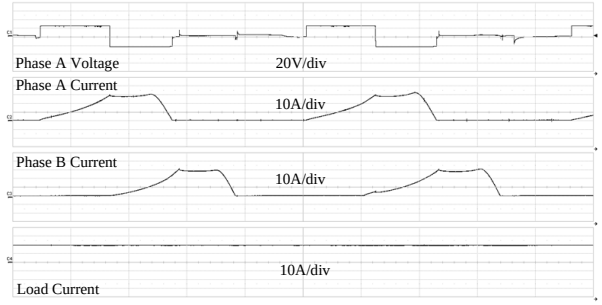

(a) Case i: i_{max} = 30 A, θ_{on} = -7.2°, θ_{off} = 8.8°, and I_L = 18.8 A, and u = 24.2 V

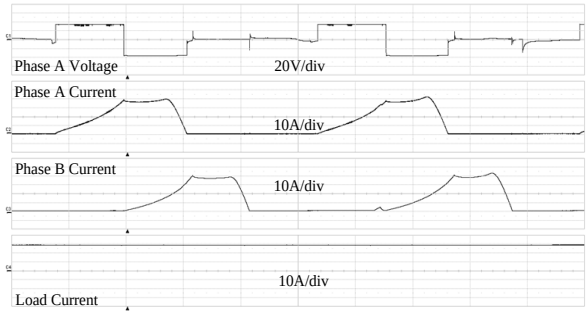

(b) Case ii: i_{max} = 40 A, θ_{on} = -7.8°, θ_{off} = 9°, and I_L = 26.8 A, and u = 36.1 V

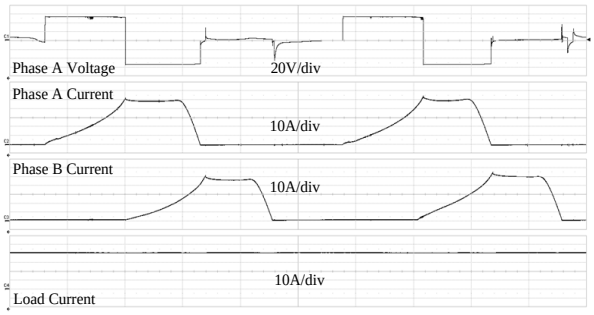

(c) Case iii: i_{max} = 50 A, θ_{on} = -8.4°, θ_{off} = 9.2°, and I_L = 38.2 A, and u = 48.2 V

Fig. 21. Three cases of waveform of phase current, when the SRG is controlled using the control variables obtained by measurement.

The phase current shape in all cases is flat-topped and the maximum output power is produced because the SRG is controlled using the optimal control variables. These results confirm the validity of the proposed analytical model.

The values of the dc bus voltage, load current, and output power for all three cases are summarized in Table 7. The output power obtained from the analytical model is different from the measurements by an average of 3.49%.

Table 7: Output power obtained from analytical model and by measurement

Case	Mathematical Model			Measurement		
	u (V)	I_L (A)	P_{out} (W)	u (V)	I_L (A)	P_{out} (W)
i	24	19.59	470.2	24.2	18.8	454.9
ii	36	27.8	1000.8	36.1	26.8	967.5
iii	48	39.76	1908.5	48.2	38.2	1841.2

The value of the current obtained from the analytical model is more than the value of the current obtained from the measurement. Since the resistance of the phase windings in the analytical model is neglected. Considering the output power based on (6), the key factor used to calculate is the current. Consequently, the output power obtained from the measurement is slightly less than the output power obtained from the analytical model. The efficiency of the system depends on the system's losses. The main losses of the system are copper loss and iron loss. The copper loss based on (7), the significant factor used to calculate is the current. The iron loss based on (9) depending on the flux linkage, the key factor used to calculate the flux linkage is the current. Therefore, the result obtained from the analytical model is different from the measurements.

VI. CONCLUSION

In this paper, the proposed inductance model applied from the flux linkage function is divided into three regions depending on the phase current and rotor position. It requires the geometrical parameters of an SRG at aligned and unaligned rotor positions. The parameters are easily quantified using the FEM. The characteristics of the inductance curve obtained using the proposed model compared with the FEM are closely matched. This result confirms the validity of the proposed model. The phase current model proposed in this paper is derived from the phase voltage equation in combination with the proposed inductance model. The shape of phase current obtained from the analytical model is also corresponding with the measurements. The optimal shape of phase current is investigated. Finally, a method to obtain the optimal control variables to maximize the output power for SRGs in single pulse mode operation is proposed. The optimal shape of the phase current is used to determine the optimal control variables. An 8/6 SRG experimental setup is used to verify the proposed method. Regarding to the results, the SRG can generate the maximum output power when the proposed optimal control variables are applied. The output power obtained from the analytical model is slightly different from the measurements. Therefore, the proposed method is accurate and reliable.

REFERENCES

[1] B. Fahimi, A. Emadi, and R. B. Sepe, "A switched reluctance machine-based starter/alternator for more electric cars," *IEEE Trans. Energy Conversion*, vol. 19, no. 1, pp. 116-124, Mar. 2004.

[2] N. Schofield and S. Long, "Generator operation of a switched reluctance starter/generator at extended speeds," *IEEE Trans. Vehicular Technology*, vol. 58, no. 1, pp. 48-56, Jan. 2009.

[3] S. R. Macminn and W. D. Jones, "A very high speed switched-reluctance starter-generator for aircraft engine applications," *in Proc. Conf. Aerospace and Electronics*, pp. 1758-1764, 1989.

[4] C. A. Ferreira, S. R. Jones, W. S. Heglund, and W. D. Jones, "Detailed design of a 30-kW switched reluctance starter/generators system for a gas turbine engine application," *IEEE Trans. Industry Applications*, vol. 31, no. 3, pp. 553-561, May 1995.

[5] R. Cardenas, W. F. Ray, and G. M. Asher, "Switched reluctance generators for wind energy applications," *in Proc. Conf. Power Electronics Specialists*, pp. 559-564, 1995.

[6] M. Ziapour, E. Afjei, and M. Yousefi, "Optimum commutation angles for voltage regulation of a high speed switched reluctance generator," *in Proc. Conf. Power Electronics, Drive Systems and Technology*, pp. 271-276, 2013.

[7] P. Asadi and B. Fahimi, "Design and control characterization of switched reluctance generator for maximum output power," *in Proc. Conf. Applied Power Electronics*, pp. 1639-1644, 2006.

[8] P. Kerdtuad and S. Kittiratsatcha "Modeling of a switched reluctance generator using cubic spline coefficients on the phase flux linkage, inductance and torque equations," *Advances in Electrical and Computer Engineering*, vol. 15, no. 1, pp. 41-48, 2015.

[9] D. W. Choi, S. I. Byun, and Y. H. Cho, "A study on the maximum power control method of switched reluctance generator for wind turbine," *IEEE Trans. Magnetics*, vol. 50, no. 1, article: 4003004, Jan. 2014.

[10] H. Chen and Z. Shao, "Turn-on angle control for switched reluctance wind power generator system," *in Proc. Conf. Industrial Electronics Society*, pp. 2367-2370, 2004.

[11] S. Yilmaz and D. A. Torrey, "Closed loop control of excitation parameters for high speed switched-reluctance generators," *IEEE Trans. Power Electronics*, vol. 19, no. 2, pp. 335-362, Mar. 2004.

[12] I. Kioskeridis and C. Mademlis, "Optimal efficiency control of switched reluctance generators," *IEEE Trans. Power Electronics*, vol. 21, no. 4, pp. 1062-1072, July 2006.

[13] S. Yu, F. Zhang, D. H. Lee, and J. W. Ahn, "High efficiency operation of a switched reluctance generator over a wide speed range," *Journal of Power Electronics*, vol. 15, no. 1, pp. 123-130, 2015.

[14] S. Wongguokoon and S. Kittiratsatcha, "Analysis of a switched-reluctance generator for maximum energy conversion," *in Proc. Conf. Sustainable Energy Technologies*, pp. 125-129, 2008.

[15] P. Thongprasri and S. Kittitratsatcha, "Optimal excitation angles of a switched reluctance generator for maximum output power," *Journal of Electrical*

Engineering and Technology, vol. 9, no. 5, pp. 1527-1536, 2014.

[16] K. N. Srinivas and R. Arumugam, "Dynamic characterization of switched reluctance motor by computer-aided design and electromagnetic transient simulation," *IEEE Trans. Magnetics*, vol. 39, no. 3, pp. 1806-1812, May 2003.

[17] S. A. Hossain and I. Husain, "A geometry based simplified analytical model of switched reluctance machines for real-time controller implementation," *IEEE Trans. Power Electronics*, vol. 18, no. 6, pp. 1384-1389, Nov. 2003.

[18] C. Roux and M. M. Morcos, "On the use of a simplified model for switched reluctance motors," *IEEE Trans. Energy Conversion*, vol. 17, no. 3, pp. 400-405, Sep. 2002.

[19] H. P. Chi, R. L. Lin, and J. F. Chen, "Simplified flux-linkage model for switched-reluctance motors," *in Proc. Electric Power Applications*, pp. 577-583, 2005.

[20] M. Stiebler and K. Liu, "An analytical model of switched reluctance machines," *IEEE Trans. Energy Conversion*, vol. 14, no. 4, pp. 1100-1107, Dec. 1999.

[21] D. A. Torrey, "Switched reluctance generators and their control," *IEEE Trans. Industrial Electronics*, vol. 49, no. 1, pp. 3-14, Feb. 2002.

[22] P. N. Materu and R. Krishan, "Estimation of switched reluctance motor loses," *IEEE Trans. Industry Applications*, vol. 28, no. 3, pp. 668-679, June 1992.

[23] P. Rafajdus, V. Hrabovcova, and P. Hudak, "Investigation of losses and efficiency in switched reluctance motor," *in Proc. Conf. Power Electronics and Motion Control*, pp. 296-301, 2006.

[24] S. Yu, D. H. Lee, and J. W. Ahn, "Efficiency analysis of switched reluctance generator according to current shape under rated speed," *Journal of International Conference on Electrical Machines and Systems*, vol. 2, no. 4, pp. 491-497, Nov. 2013.

[25] R. L. Lin, J. F. Chen, and H. P. Chi, "Spice-based flux-linkage model for switched reluctance motors," *in Proc. Conf. Electric Power Applications*, pp. 1468-1476, 2005.

[26] M. Krishnamurthy, B. Fahimi, and C. S. Edrington, "On the measurement of mutual Inductance for a switched reluctance machine," *in Proc. Conf. Power Electronics Specialists*, pp. 1-7, 2006.

[27] H. K. Bae and R. Krishnan, "A novel approach to control of switched reluctance motors considering mutual inductance," *in Proc. Conf. Industrial Electronics Society*, pp. 369-374, 2000.

Pairote Thongprasri He received his M.Eng. degree in Electrical Engineering from KMITL. He is studying in D.Eng. program (Electrical Engineering) at KMITL. His research interests are switched reluctance machine and power electronics.

Supat Kittiratsatcha received his M.S. and Ph.D. degrees in Electric Power Engineering from Rensselaer Polytechnic Institute, Troy, NY. He is an Associate Professor with the Department of Electrical Engineering at KMITL. His research interests include switched reluctance machine design and solid state lighting.